

# Desensitizing The Pin-Point Landing Trajectory On Mars

Haijun Shen, Hans Seywald, Richard W. Powell\*  
*Analytical Mechanics Associates, Inc.*  
*Hampton, VA*

## Abstract

This paper describes the first phase of an effort to demonstrate the use of Desensitized Optimal Control (DOC) methodology to develop an optimal Mars Entry, Descent, and Landing (EDL) trajectory. DOC methodology is developed based on the conventional optimal control formulation except that the original objective function is augmented with the sensitivity of a given function with respect to state perturbations encountered along the trajectory. The result is an optimal trajectory with reduced sensitivity of the given quantity with respect to the state perturbations, but without an excessive compromise in terms of the original objective value. The presence of perturbations such as the deviation of the spacecraft at the atmospheric interface from the desired entry position, atmospheric density uncertainties, winds, etc., could greatly compromise the landing precision. Thus, it is the goal of this study to reduce the sensitivity of the landing errors with respect to the perturbations. In this paper, only the entry portion of the EDL trajectory from the atmospheric interface to the parachute deployment is considered, and the initial position error at the entry are considered as the only perturbations. It aims at reducing the sensitivity of the position at the parachute deployment with respect to the entry position error, while minimizing the fuel consumption. It is assumed that the spacecraft flies at a constant angle of attack, and the only control authority is the banking of the spacecraft.

## Nomenclature

|                       |  |                              |   |
|-----------------------|--|------------------------------|---|
| $r_m$                 | Radius of Mars   | $h$                          | Altitude  |
| $\phi$                | Latitude   | $\theta$                     | Longitude   |
| $v_r$                 | Radial velocity  | $v_n$                        | Northward velocity  |
| $v_e$                 | Eastward velocity  | $\mu$                        | Gravitational parameter of Mars   |
| $a_r$                 | Radial acceleration of the lift and drag forces acting on the lander   | $a_n$                        | Northward acceleration of the lift and drag forces acting on the lander |
| $a_e$                 | Eastward acceleration of the lift and drag forces acting on the lander | $\xi$                        | Bank angle  |
| $u$                   | Bank acceleration  | $\mathcal{J}_0, \mathcal{J}$ | Nominal and augmented objective functions                               |
| $T$                   | Temperature  | $P$                          | Pressure  |
| $\rho$                | Atmospheric density  | $I$                          | Identity matrix   |
| $\mathcal{S}(t, t_0)$ | Sensitivity matrix of states at $t$ with respect to states at $t_0$    | $(\cdot)^T$                  | Matrix transposition  |
| $y$                   | State vector   | $f(\cdot)$                   | Right-hand side of the system dynamics                                  |

## 1 Introduction

The landing accuracy is vital to many Mars exploration missions. However, accurate landing faces steep challenges. For example, the atmosphere is thick enough to create sufficient heating, but not enough for a low terminal descent velocity; the atmosphere varies (density, winds, etc.) unpredictably, and it is not as well-studied as the Earth atmosphere; the Mars surface environment is made of complex rocks, craters, dust and terrain patterns, and it is costly to replicate a Mars relevant environment for space flight qualification to test entry, descent, and landing (EDL) technologies [1], etc. In fact, non-guided entry trajectories have been flown in all of the past Mars missions. The Mars Surveyor Program 2001 (MSP'01), although not flown, was the first mission planned for an actively guided entry [2, 3, 4, 5, 6]. The goal was to reduce the 3- $\sigma$  landing footprint by one order of magnitude from the 280 km by 100 km footprint ellipse of

\*shen@ama-inc.com; seywald@ama-inc.com; richard.w.powell@nasa.gov

the Pathfinder program. In 2010, a next generation EDL systems is planned for the Mars Science Laboratory (MSL) mission, delivering the largest and most capable rover to date to the surface of Mars. MSL will fly a guided lifting entry with a lift-to-drag (L/D) ratio in excess of that ever flown at Mars [7]. High-fidelity flight simulations have shown that the MSL is capable of having a  $3\text{-}\sigma$  footprint of about 10 km radius.

One technique developed for reducing the landing error is the ‘‘Smart Chute’’ scheme [8]. ‘‘Smart Chute’’ refers to the fact that the parachute will be deployed when the position of the spacecraft is closest to the planned hand-off location to the descent phase. Since the altitude and the velocity are not taken into consideration of the ‘‘Smart Chute’’ guidance command, guard bands must be used to ensure that the parachute is not deployed at an altitude which is too low or with a load which is too high. Clearly, the ‘‘Smart Chute’’ technique alleviates the requirement that the spacecraft precisely hits the desired parachute deployment point, especially in the downrange direction. However, as limitations exist for the ‘‘Smart Chute’’ technique, the success of a precision landing still intimately depends on the guidance of the entry spacecraft. In addition, the ‘‘Smart Chute’’ technique may put extra requirement on the design of the parachute to endure a larger range of loads.

In all these EDL system design and simulations, limited sensitivity information of the trajectory to the perturbations and uncertainties on the flight conditions is considered. Examples of such perturbations and uncertainties are entry position errors, navigation errors, the wind variations, atmosphere density variations, etc. Each of these perturbations and uncertainties increases the challenge of reducing the landing footprint [1]. In addition, little effort is spent on minimizing the fuel consumption. Reference [4] resembles this study the most among the existing guidance designs [3, 4, 5, 6], but the sensitivity of the vehicle response to perturbations is treated mostly on a trial-and-error basis, and no conservation of fuel consumption is considered in the guidance design.

This study aims at filling the gap by developing an EDL trajectory with reduced sensitivity of landing position with respect to perturbations and uncertainties and least possible fuel consumption. The reduced sensitivity would lead to further reduction of landing ellipse. This is achieved by employing the Desensitized Optimal Control (DOC) methodology [9]. DOC is based on the traditional optimal control formulation which includes system dynamics, constraints, boundary conditions, and an objective function, etc., with the addition of the dynamics of the sensitivity of the states at any time with respect to the state at initial time. To also reduce the sensitivity of a given function with respect to perturbations, the original objective function is augmented with the sensitivity through a weighting factor. As a result, this leads to a trajectory which is an optimally weighted balance between the original objective and the added objective of reducing the sensitivity. DOC has been applied successfully in the rocket landing problem [10] and low-thrust interplanetary trajectory designs [11], etc.

In this paper, only the entry portion of the EDL is considered (from the atmospheric interface to the parachute deployment). It is assumed that the entry vehicle is not exactly placed at the desired entry position at the atmospheric interface, and the corresponding deviation is considered as the sole source of perturbations. The goal is to reduce the position error from the desired parachute deployment point as a result of the initial position error, with a minimal level of fuel consumption. It is also assumed that the spacecraft is commanded to fly at a constant angle of attack, and the controlled guidance of the vehicle is achieved only through modulating the bank angle of the entry vehicle with an RCS system.

This paper is organized in the following fashion. Following the Introduction section is the section describing the equations of motion of the entry spacecraft as well as the atmospheric density model used in this study. Then the formulation of the DOC methodology is described. The simulation results will be presented next, followed by some discussion and the conclusion.

## 2 Equations of Motion

The equations of motion of the entry vehicle are presented in this section. The position of the entry vehicle is represented by its altitude  $h$ , latitude  $\phi$  and longitude  $\theta$ . Its velocity is represented by the radial velocity  $v_r = \dot{h}$ , the northward velocity  $v_n = (r_m + h)\dot{\phi}$ , and the eastward velocity  $v_e = (r_m + h)\dot{\theta}\cos\phi$ , where  $r_m$  stands for the radius of the Mars. Let  $a_r$ ,  $a_n$  and  $a_e$  denote the radial, northward, and eastward acceleration resulting from the aerodynamic drag and lift forces acting on the entry vehicle. Then, the trajectory of the entry vehicle is governed by the following

equations of motion.

$$\begin{aligned}
\dot{h} &= v_r \\
\dot{\phi} &= \frac{v_n}{r_m + h} \\
\dot{\theta} &= \frac{v_e}{(r_m + h) \cos \phi} \\
\dot{v}_r &= -\frac{\mu}{(r_m + h)^2} + \frac{v_n^2 + v_e^2}{r_m + h} + a_r \\
\dot{v}_n &= -\frac{v_r v_n + v_e^2 \tan(\phi)}{r_m + h} + a_n \\
\dot{v}_e &= -\frac{v_r v_e - v_n v_e \tan(\phi)}{r_m + h} + a_e
\end{aligned} \tag{1}$$

The attitude of the vehicle is controlled using a reaction control system. For this analysis, the angle of attack is kept constant. Any control of the entry trajectory is achieved solely through modulating the bank angle  $\xi$  of the entry vehicle, which is driven by the following dynamic equation.

$$\ddot{\xi} = u, \tag{2}$$

where  $u$  is the angular acceleration as a result of the bank angle reaction control system. As mentioned above, the control accelerations  $a_r$ ,  $a_n$ , and  $a_e$  is modulated by the bank angle  $\xi$ . The bank rate and bank acceleration are both constrained with prescribed bounds; i.e.,

$$\dot{\xi}_{\min} \leq \dot{\xi} \leq \dot{\xi}_{\max}, \text{ and } u_{\min} \leq u \leq u_{\max}.$$

The objective for the nominal trajectory (absent of perturbations) is to minimize the fuel consumption which is approximately proportional to the cumulative bank rate expressed as  $\int_{t_0}^{t_f} |u(t)| dt$ . However, since the control appears linearly in the equations of motion, the optimization leads to the well-known bang-coast-bang solution. This may pose numerical difficulties when using collocation methodology because of possible appearance of chattering control. In addition, the control being at its bounds may cause difficulties in practice in using feedback laws to track the optimal solution because the feedback control could be outside the prescribed bounds. Therefore, a more numerically benign objective function, the control energy, is chosen, which can be written as

$$\min_{u(t)} \mathcal{J}_0 = \int_{t_0}^{t_f} u(t)^2 dt \tag{3}$$

For practical purposes, the fuel consumption obtained by minimizing  $\mathcal{J}_0$  is not too far off the minimum fuel consumption.

This paper considers only the entry portion of the EDL trajectory. Thus,  $t_0$  stands for the time at the atmospheric interface, and  $t_f$  the time at the parachute deployment. A simple atmospheric model of Mars is adopted in this study. It is obtained by curve-fitting a data set consisting of temperature, pressure, and density, produced by MarsGRAM program. The following equations describe the atmospheric model used in this study.

$$\begin{aligned}
T &= 1.4 \times 10^{-13} h^3 - 8.85 \times 10^{-9} h^2 - 1.245 \times 10^{-3} h + 205.3645 \\
P &= 559.351005946503 e^{-0.000105h} \\
\rho &= \frac{P}{188.95110711075 T}
\end{aligned} \tag{4}$$

where  $h$  is in meters, density  $\rho$  in  $\text{kg/m}^3$ , temperature  $T$  in Kelvin, and pressure  $P$  in  $\text{N/m}^2$ .

### 3 Desensitized Optimal Control Formulation

In reality, the trajectory flown for an actual mission is never the nominal trajectory planned, as there are always uncertainties and perturbations along the trajectory. The purpose of the DOC methodology is to reduce the sensitivity

of a given function with respect to the uncertainties and perturbations. A full explanation of DOC is given in Ref. [9]. In this paper, we assume that the spacecraft is not placed exactly at the planned entry position at the atmospheric interface, and consider the initial position error as the only source of perturbations along the entry trajectory. The initial position error, if not properly attenuated, will be propagated and magnified to a larger position error at the parachute deployment point, which eventually will cause large position errors at the landing point. Thus, in an attempt to place the spacecraft as closely to the planned parachute deployment point as possible, this study minimizes the sensitivity of the final position at the parachute deployment with respect to the initial position error at the entry, while still taking into consideration the original objective of minimizing the control energy.

In Eqs. (1) and (2), let  $y$  denote the state vector, and  $f(y, u, t)$  denote the right-hand side. Furthermore, let  $\mathcal{S}(t, t_0)$  denote the sensitivity of the state vector at time  $t$  with respect to the state vector at initial time  $t_0$ . Then, according to Ref. [9],  $\mathcal{S}(t_0, t_0) = I$ , and  $\mathcal{S}(t, t_0)$  satisfies the following differential equation.

$$\dot{\mathcal{S}}(t, t_0) = \left( \frac{\partial f}{\partial y} + \frac{\partial f}{\partial u} \cdot K \right) \cdot \mathcal{S}(t, t_0) \quad (5)$$

where  $K$  is the feedback gain which dictates what trajectory the spacecraft should fly (in the neighborhood of the nominal trajectory) once the perturbation is encountered. Specifically, the control of the perturbed trajectory is defined by the following linear feedback law:

$$u(t) = u^*(t) + K(t) \cdot (y(t) - y^*(t))$$

where  $u^*(t)$  and  $y^*(t)$  denote the control and state vectors of the nominal trajectory at time  $t$ . The feedback control gain  $K$  can be prescribed by the user, be treated as fixed constants to be optimized, or be treated as additional time-varying control variables subject to user-specified bounds.

According to the standard DOC approach, the goal mentioned above can be achieved by augmenting the original objective function  $\mathcal{J}_0$  with the sensitivity of the final position with respect to the initial position error. That is, the augmented objective function takes on the following form,

$$\mathcal{J} = \mathcal{J}_0 + c_1 \cdot \|\mathcal{S}_p(t_f, t_0, K)\|_F \quad (6)$$

where  $c_1$  is a positive weighting factor, and  $\|\mathcal{S}_p\|_F = \sqrt{\text{trace}(\mathcal{S}_p \cdot \mathcal{S}_p^T)}$  stands for the Frobenius norm of matrix  $\mathcal{S}_p$ . Let position variables  $h$ ,  $\phi$ , and  $\theta$  be the first three element of the position vector  $y$ , then  $\mathcal{S}_p$  represents the upper left  $3 \times 3$  block of the sensitivity matrix  $\mathcal{S}$ .

With the sensitivity dynamics in Eq. (5) and the new objective function in Eq. (6), the DOC methodology will yield a different optimal trajectory from the one without the sensitivity consideration; i.e., the optimal trajectory is “reshaped” to a less sensitive one in terms of the considered sensitivity. Not surprisingly, the original objective function  $\mathcal{J}_0$  associated with the desensitized trajectory has a larger value than that of the optimal trajectory without the sensitivity consideration. The value of the weighting factor  $c_1$ , along with the feedback gain vector  $K$ , affects how the optimal trajectory is reshaped.

## 4 Numerical Results

The entry vehicle selected for this study has similar specifications as an earlier MSL concept. It is a 70 degree sphere cone aeroshell, and the parameters of the vehicle relevant to this study are summarized in Table 1. It is assumed that the entry vehicle maintains a constant trim angle of attack of 11 degrees. As in MSL, the entry vehicle is commanded to various bank angles to modulate the desired lift profile, and thus, to achieve the desired trajectory. In addition, the reaction control system poses physical limitations on the banking ability of the entry vehicle. Specifically, the bank acceleration cannot exceed  $\pm 5 \text{ deg/s}^2$ , the bank rate cannot exceed  $\pm 20 \text{ deg/s}$ , and the bank angle is not bounded. In terms of the optimal control formulation, the two bounds on the bank acceleration and bank rate are treated as a control constraint and a state constraint, respectively. The initial conditions are given as the planned altitude, velocity and flight path angle of the spacecraft at the time it enters the Mars atmosphere; the terminal conditions are prescribed by the desired parachute deployment conditions. The boundary conditions used in this study are summarized in Table 2.

Table 1: Parameters associated with the entry vehicle

|                             |                        |
|-----------------------------|------------------------|
| Aeroshell diameter          | 4.6 m                  |
| Ballistic Coefficient       | 115 kg/m <sup>2</sup>  |
| L/D ratio                   | 0.18                   |
| Roll moment of inertia      | 5000 kg·m <sup>2</sup> |
| Yaw moment of inertia       | 4000 kg·m <sup>2</sup> |
| Roll moment arm             | 1.25 m                 |
| Yaw moment arm              | 1 m                    |
| Specific impulse of the RCS | 215 s                  |

Table 2: Initial and final conditions of the entry trajectories

| Parameters        | At atmospheric interface | At parachute deployment |
|-------------------|--------------------------|-------------------------|
| altitude          | 126.1 km                 | 10 km                   |
| velocity          | 6750 m/s                 | 503 m/s                 |
| longitude         | 0 deg                    | 12.2 deg                |
| latitude          | 0 deg                    | 0 deg                   |
| flight path angle | -15.2 deg                | Not prescribed          |

EZopt<sup>®</sup>\*, which employs the direct method, is used to solve the optimal control problem. An integrated tool is also developed so that the DOC methodology is completely incorporated within the EZopt platform. The software package enables two direct methods, namely, differential inclusion [12] and collocation [13]. In this study, the collocation scheme with 101 equally-distanced nodes is used.

The nominal trajectory with no DOC consideration is obtained by minimizing the objective function in Eq. (3). Figure 1(a) shows the bank rate and acceleration, and Fig. 1(b) shows the bank angle. The nominal trajectory consists of two bank reversals, and the bank rate and bank acceleration remain within their bounds,  $\pm 20$  deg/s and  $\pm 5$  deg/s<sup>2</sup>, respectively. This solution will be referred to as the no-DOC solution in this paper. Clearly, the no-DOC solution is also obtained by setting  $c_1 = 0$  in Eq. (6). Starting with  $c_1 = 0$ , and then slowly increasing  $c_1$ , DOC solutions can be generated through homotopies, and the effect of putting more emphasis on the reduction of sensitivities on the overall shape of the trajectory can be observed.

In the following, trajectories as results of DOC methodology will be presented. The radius, downrange, and crossrange channels will be examined and presented separately. It can be seen from the boundary conditions that the planned entry point and the prescribed target point both lie within the equatorial plane. Thus, the downrange is represented by the longitude variable, and the crossrange is represented by the latitude variable.

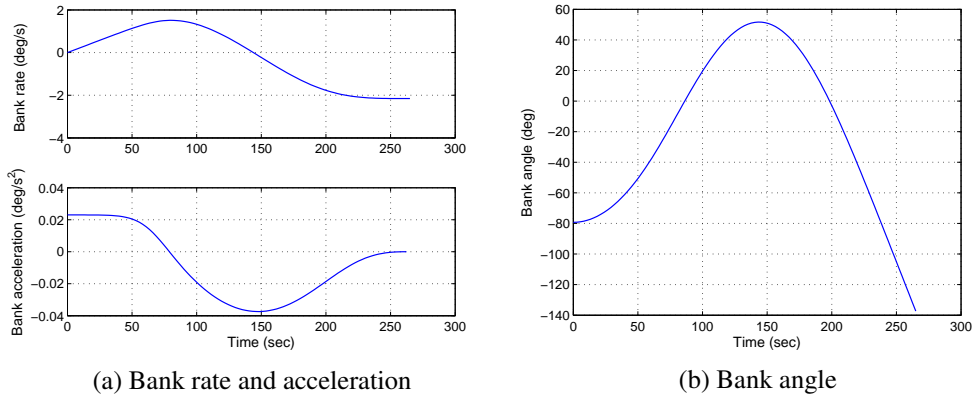


Figure 1: Bank rate, acceleration, and bank angle of the nominal no-DOC trajectory.

\*EZopt<sup>®</sup> software was developed by AMA under NASA SBIR funding.

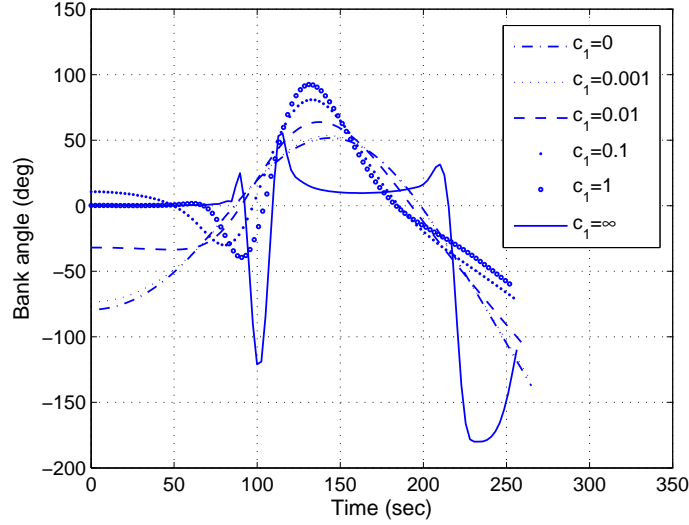


Figure 2: Bank angle profiles of the desensitized solutions for various  $c_1$ .

#### 4.1 The Radius Channel

One of the virtues of the DOC methodology is that it can reshape the nominal trajectory such that the desired sensitivity is reduced along the new nominal trajectory, even without the help of the feedback gain (with  $K = 0$  in Eq. (5)). However, there are limitations on how much the sensitivity can be reduced, which depends on the physics of the problem, as well as the weighting factor  $c_1$  in the augmented objective function in Eq. (6). In addition, the reduction of the sensitivity is achieved at the expense of the original objective function in Eq. (3). This subsection examines the reduction of the sensitivity of the final position with respect to initial radius error, and first, the focus is placed on the case where the feedback gain  $K$  is a zero vector. Using the aforementioned method with homotopies, desensitized trajectories are obtained for various values of the weighting factor  $c_1$ . The corresponding bank angle profiles are shown in Fig. 2, and the bank angle evolving with  $c_1$  shows that the reshaping of the nominal trajectories is evident.

Typically, compared with the no-DOC solution, a desensitized trajectory spends more time in lower altitude where the atmosphere has a higher density, and has more bank reversals, resulting in a higher fuel consumption. Table 3 tallies the fuel consumption of each of the nominal trajectories and the final position errors as a result of an initial radius error of 1000 m. For reference, the value of the objective function  $J_0$  and the cumulative bank rate for each case are also shown in Table 3. Notice that the case where  $c_1 = 0$  is the same as the nominal no-DOC solution. It can be seen from Table 3 that along the nominal no-DOC solution, an initial radius error of 1000 m is magnified to 8039 m when propagated to the final time, with an objective value  $J_0=0.1374 \text{ deg}^2/\text{s}^3$ , and the associated fuel consumption is 0.204 kg. Not surprisingly, the optimal no-DOC trajectory ( $c_1 = 0$ ) has the smallest value of  $J_0$ , but has the largest sensitivity of the final position with respect to the initial radius error. As  $c_1$  increases gradually, more and more emphasis is placed on the augmenting objective function, and the final position error is reduced, accompanied by the increase of  $J_0$ . Notice also that increasing  $J_0$  translates into increasing fuel consumption except when  $c_1$  changes from 0 to 0.001. The discrepancy is due to the fact that the minimum control energy ( $J_0$ ) is not an exact representation of the minimum fuel consumption. The smallest final position error one can obtain is 5939 m (a 26.1% reduction from 8039 m) when placing all emphasis on reducing the sensitivity by setting  $c_1 = \infty$ , and the associated fuel consumption is almost 33 times that of the nominal no-DOC case.

In light of Table 3, it can be seen that just by reshaping the nominal trajectory is not enough to bring the sensitivity down to a satisfactory level. Therefore, more degrees of freedom is needed to reduce the sensitivity. To this end, feedback gains are introduced which could help bring the perturbed trajectory to a smaller target hitting error.

In this paper, the feedback gains are considered constant and not time-varying. Making the gains time-varying introduces further degrees of freedom in reducing the target hitting errors. In addition, it is assumed that the position

Table 3: The fuel consumption and final position errors for various  $c_1$

| $c_1$      | $\mathcal{J}_0$ (deg <sup>2</sup> /s <sup>3</sup> ) | Cumulative bank rate | Fuel consumption | Final position error |
|------------|---|----------------------|------------------|----------------------|
| 0 (no-DOC) | 0.1374  | 5.1784 deg/s         | 0.204 kg         | 8039 m               |
| 0.001      | 0.14  | 5.1233 deg/s         | 0.202 kg         | 7959 m               |
| 0.01       | 0.3078  | 6.1277 deg/s         | 0.242 kg         | 7372 m               |
| 0.1        | 1.5603  | 12.8236 deg/s        | 0.506 kg         | 6472 m               |
| 1.0        | 5.1812  | 20.5832 deg/s        | 0.812 kg         | 6172 m               |
| $\infty$   | 586.8673  | 166.9280 deg/s       | 6.583 kg         | 5939 m               |

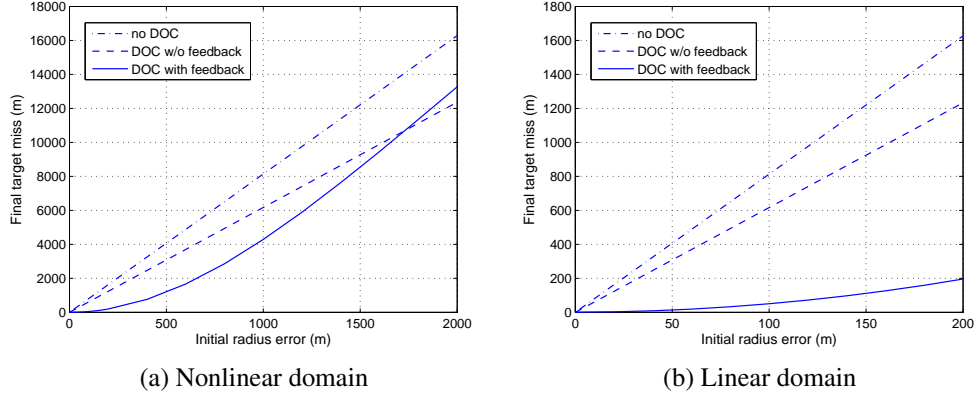


Figure 3: Target hitting errors resulting from various initial radius errors.

and velocity are the only available (directly measurable or observable) states for feedback. Using the nominal no-DOC solution as the starting point, it was possible to obtain a trajectory along which the sensitivity of the target hitting error with respect to the initial radius error is greatly reduced. The comparisons of the no-DOC solution, no-feedback DOC solution with  $c_1 = 1$ , and the with-feedback DOC solution are presented in Figs. 3, 4 and 5. Figure 3 shows the position errors at the final time resulting from various initial radius errors. It clearly illustrates the smaller target hitting error of the no-feedback DOC solution compared with the no-DOC solution. Because the sensitivity dynamics in Eq. (5) is based on linearization of the system dynamics, the reduction of sensitivity can only be observed for perturbations in the domain where the linearization is valid. It can be seen from Fig. 3(a) that the the no-DOC and no-feedback DOC solutions have much larger linear domain than the with-feedback solution, but the with-feedback DOC solution shows significantly more reduction of the final target hitting error for smaller initial radius errors in the linear domain. A zoom-in plot of the final target hitting error in the linear domain is shown in Fig. 3(b).

Figure 4 shows the comparison of the final target hitting error histories between the no-DOC, the no-feedback DOC, and the with-feedback DOC solutions, given an initial radius error of 200m. Figure 5 shows the comparison between the bank angles, the bank rates, and the bank accelerations of the nominal with-feedback DOC trajectory and the perturbed trajectory with feedback with the same initial radius error. It should be pointed out that the solid lines in both Figs. 4 and 5 correspond to the same perturbed trajectory with feedback. It can be seen from Fig. 4 that along the nominal no-DOC trajectory, the initial radius error of 200m contributes mainly to 1600m of final downrange error, and the no-feedback DOC solution brings it down somewhat, but it is the with-feedback DOC solution that has the most impact on reducing the final target hitting error. It can be seen from Fig. 5(b) that the feedback law forces the perturbed trajectory to assume a larger reversed (negative) bank angle in the beginning of the trajectory (from 0s to 100s) than the nominal values. That causes the perturbed trajectory to assume a larger crossrange deviation and a faster reduction in the radius compared with the unperturbed nominal trajectory, as evident in Fig. 4. The faster reduction in radius brings the spacecraft to an area of the atmosphere with higher density, and the resulting larger drag helps reduce the downrange deviation. During the middle portion of the trajectory (from 100s to 200s), the perturbed trajectory assumes a larger positive bank angle than the nominal values, which would cause further reduction in the radius and downrange, but effectively corrects the crossrange error. In the remaining portion of the trajectory, the perturbed trajectory assumes a smaller reversed bank angle, which causes a larger lift profile and a smaller drag profile

than the nominal trajectory, and thus corrects the remaining radius and downrange error.

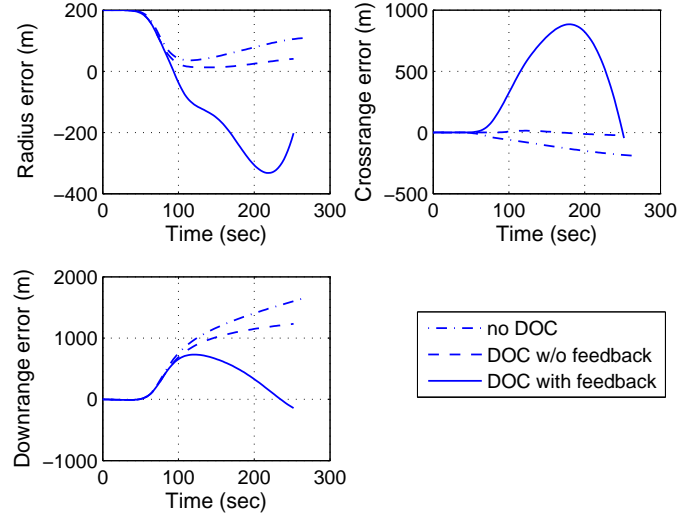


Figure 4: Time history of position errors, due to initial radius error of 200m.

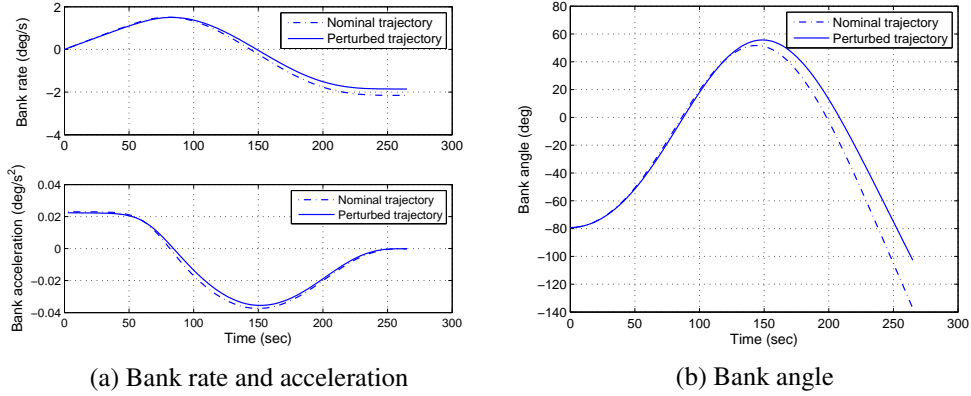


Figure 5: Time history of bank angle, rate, and acceleration, due to initial radius error of 200m.

Figure 5(a) shows that the perturbed trajectory and the nominal trajectory have comparable bank acceleration levels, and thus, the feedback law does not introduce excessive amount of extra fuel consumption.

## 4.2 The Downrange Channel

As pointed out previously, the DOC approach is capable of reshaping the nominal trajectory such that the sensitivity of a selected metric with respect to state perturbations along the nominal trajectory is minimized. However, this is not always the case without incorporating the feedback gains. This section will show that without feedback gains, DOC approach is incapable of reducing the sensitivity of the terminal position with respect to the initial downrange error. To this end, since there are no feedback gains, Eq. (5) becomes

$$\dot{S}(t, t_0) = \frac{\partial f}{\partial y} \cdot S(t, t_0) \quad (7)$$

Notice that since the downrange variable  $\theta$  does not appear explicitly in the right hand side of the system dynamics in Eqs. (1) and (2), the third column of  $\partial f/\partial y$  takes on all zero values. According to the mid-point rule of integration

employed in the EZopt application, at each time  $t_k$ , the sensitivity matrix  $\mathcal{S}$  is updated in the following way,

$$\frac{\mathcal{S}(t_{k+1}, t_0) - \mathcal{S}(t_k, t_0)}{t_{k+1} - t_k} = \frac{\partial f}{\partial y} \cdot \frac{\mathcal{S}(t_{k+1}, t_0) + \mathcal{S}(t_k, t_0)}{2}$$

where  $\partial f/\partial y$  is evaluated at  $(t_{k+1} + t_k)/2$ . Thus,

$$\mathcal{S}(t_{k+1}, t_0) = \left( I - \frac{t_{k+1} - t_k}{2} \cdot \frac{\partial f}{\partial y} \right)^{-1} \cdot \left( I + \frac{t_{k+1} - t_k}{2} \cdot \frac{\partial f}{\partial y} \right) \cdot \mathcal{S}(t_k, t_0)$$

Given the fact that the third column of  $\partial f/\partial y$  consists of all zeros, the third columns of the first two terms of the right-hand-side of the above equation are both

$$e_3 = [0 \ 0 \ 1 \ 0 \ 0 \ 0 \ 0]^T$$

In addition,  $\mathcal{S}(t_0, t_0)$  is the identity matrix. Therefore, the third column of the sensitivity matrix  $\mathcal{S}$  at any time step will remain  $e_3$ . That is, the final target hitting error will equal to the initial downrange error if it is the only perturbation at the initial time. Although the discretization scheme is used to show that the sensitivity of the final position with respect to the initial downrange error is 1, the result holds regardless of the discretization scheme. Notice that  $e_3$  as the third column of a sensitivity matrix  $\mathcal{S}(t, t_0)$  satisfies the sensitivity dynamics in Eq. (7) and the initial condition  $\mathcal{S}(t_0, t_0) = I$ . Physically, this makes sense because if only the downrange is shifted and nothing else changes from the nominal conditions at the beginning, the perturbed trajectory will be a mere copy of the nominal trajectory with the same amount of downrange shift throughout. This is independent of the shape of the nominal trajectory.

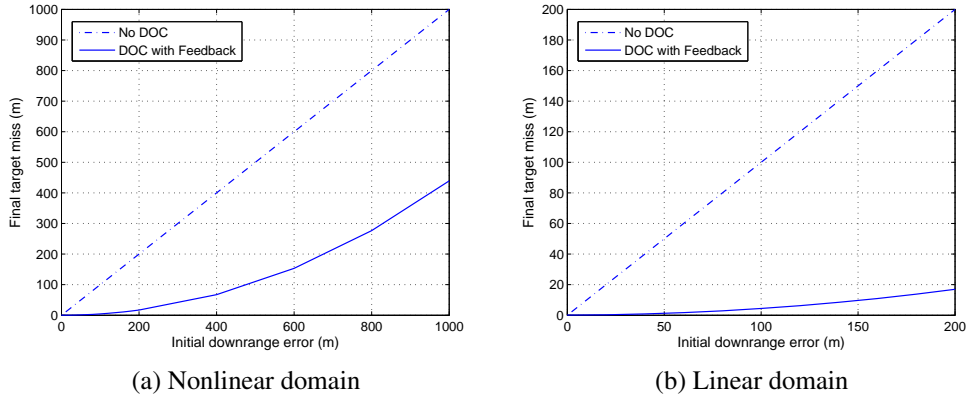


Figure 6: Target hitting errors resulting from various initial downrange errors.

In this case, feedback has to be used to annihilate the effect of the initial downrange error. In addition, the feedback has to include a non-zero gain at the downrange variable to change the third column of the sensitivity matrix. A with-feedback DOC solution is obtained, and the results are shown in Figs. 6, 7, and 8. Figure 6 shows the comparison of the final target hitting errors of the no-DOC solution and the with-feedback DOC solution resulting from various initial downrange errors. There, the sensitivity of the final position with respect to the initial downrange error along the no-DOC solution is 1, as shown analytically above, and the sensitivity is significantly reduced along the with-feedback DOC solution. For an initial downrange error of 1000m, the reduction of the final target hitting error is more than half compared with the no-DOC solution, and the reduction is even more significant for smaller initial downrange errors in the linear domain, as evident in Fig. 6(b).

Figures 7 and 8 show the comparison of the nominal trajectory and the perturbed trajectories with feedback with an initial downrange error of 200m. Figure 8 shows that if no feedback is used, the downrange error at the final time is 200m, and there are no radius and crossrange errors. Thus, the primary purpose of the feedback law is to reduce the final downrange error, while not causing excessive final radius and crossrange errors. Figure 7(b) shows that the feedback law dictates the perturbed trajectory to assume a larger reversed bank angle than the nominal values from the beginning till about  $t = 130$ s, which causes the perturbed trajectory to have a larger crossrange excursion as well as a smaller radius profile than the nominal trajectory. Flying at a lower altitude along the perturbed trajectory implies

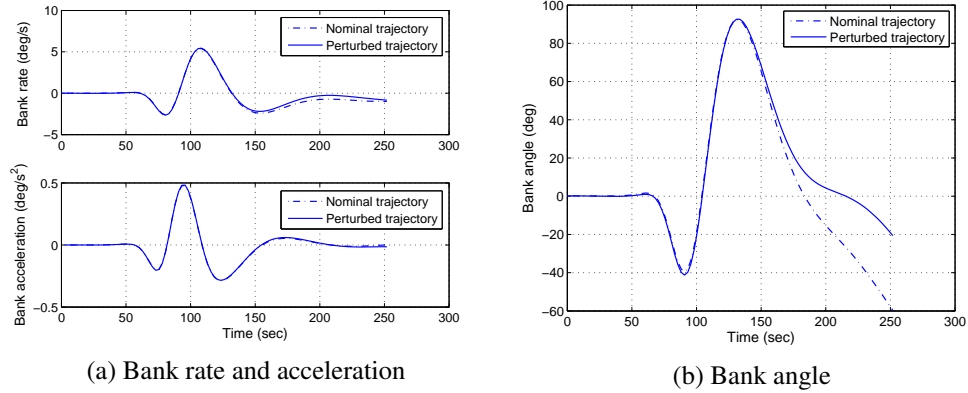


Figure 7: Bank angle, rate, and acceleration, due to initial downrange error of 200m.

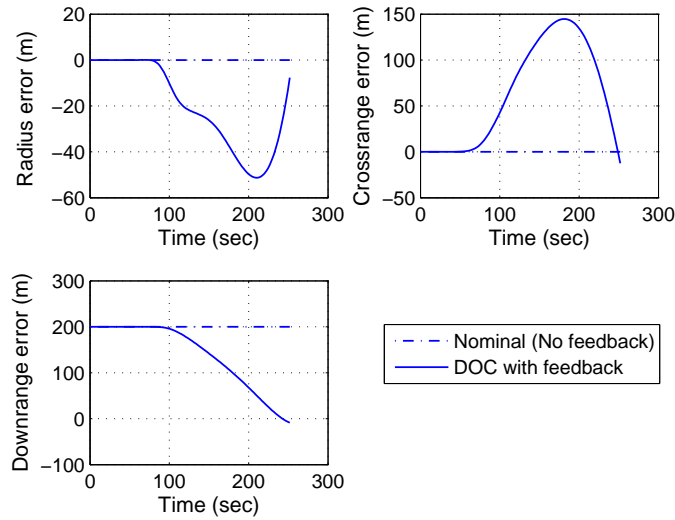


Figure 8: Time history of position errors, due to initial downrange error of 200m.

that the spacecraft is exposed to denser atmosphere than it would along the nominal trajectory, and the ensuing larger drag reduces the downrange error. After  $t = 130$ s, feedback law commands the vehicle to bank more to the positive side than the nominal banking profile, which helps correct the crossrange error. After about  $t = 200$ s, the spacecraft is commanded to a bank angle smaller than the nominal case, which creates more lift, and effectively corrects the radius error.

### 4.3 The Crossrange Channel

Similar to the downrange channel, the sensitivity of the final position with respect to the initial crossrange error cannot be reduced without feedback. A with-feedback DOC solution is obtained, and the results shown in Figs. 9, 10, and 11. The comparison of the final target hitting errors of the no-DOC solution and the with-feedback DOC solution with various initial crossrange errors is shown in Fig. 9. It can be seen that the sensitivity of the final position with respect to the initial crossrange error along the no-DOC solution is close to 1. Compared with the no-DOC trajectory, the perturbed trajectory with feedback has significantly reduced sensitivity. For an initial crossrange error of 1000m, the reduction of the final target hitting error is about twenty-fold, and the reduction is even more significant for smaller initial crossrange errors.

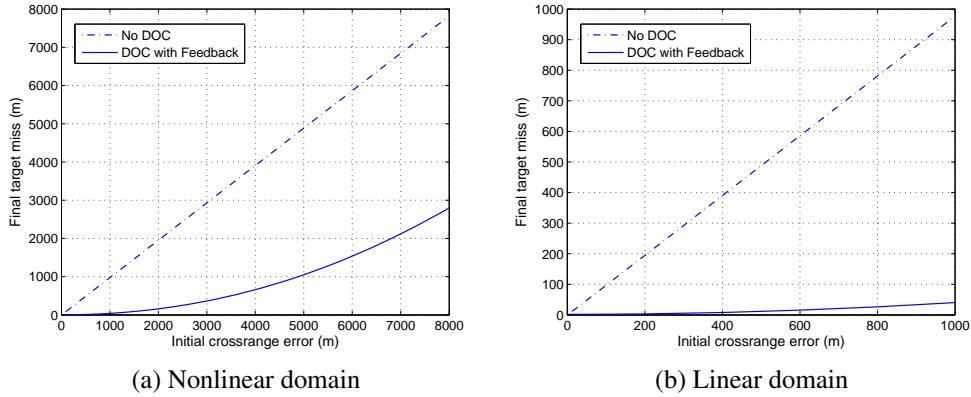


Figure 9: Target hitting errors, due to various initial crossrange errors.

Figures 10 and 11 show the comparison of the nominal trajectory and the perturbed trajectory with feedback with an initial crossrange error of 1000m. Figure 11 shows that without feedback law, an initial crossrange error of 1000m only results in a crossrange error of 1000m at the final time. Thus, the primary purpose of the feedback law is to reduce the final crossrange error, while not causing excessive final radius and downrange errors. It can be seen from Fig. 10(b) that the feedback law commands the perturbed trajectory to assume a smaller reversed bank angle than the nominal values at the beginning of the trajectory, which helps correct the positive crossrange error. A smaller reversed bank angle also implies more vertical lift than the nominal trajectory, which in turn causes the perturbed trajectory to have a larger radius and downrange profile than the nominal trajectory. When the bank angle is reversed, however, the perturbed trajectory assumes a larger positive bank angle than the nominal trajectory, which causes the positive crossrange error to continue to drop. The larger positive banking also implies smaller vertical lift than the nominal values, which in turn causes the reduction in radius and downrange. After the final reversal, the perturbed trajectory again assumes a smaller reversed bank angle, which helps correct the remaining radius and downrange errors.

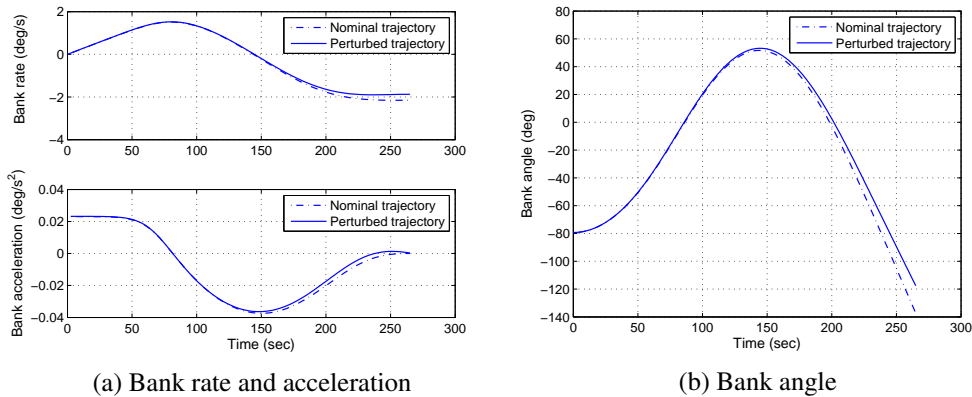


Figure 10: Time history of bank angle, rate, and acceleration, due to initial crossrange error of 1000m.

**Discussion:** It should be pointed out that the feedback control gains obtained in this paper only apply for the specific perturbation considered. In practice, one can compute feedback gains for multiple perturbations once they are identified. The fuel consumption for the nominal trajectory is much less than the MSL (MSL consumes about 9kg). However, it is noted that the lowering the sensitivity requires more fuel consumption because the desensitized trajectory typically spends more time in denser atmosphere and also has more bank reversals. Once more perturbations are considered, the fuel consumption for reducing the sensitivity will definitely rise. However, since the fuel consumption is also minimized when calculating the desensitized trajectories, the fuel consumption is not expected to exceed that of the MSL where minimizing the fuel consumption is not considered. The perturbation to be considered next is the variation of the atmosphere density. Further works also include modulating the angle of attack of the entry vehicle,

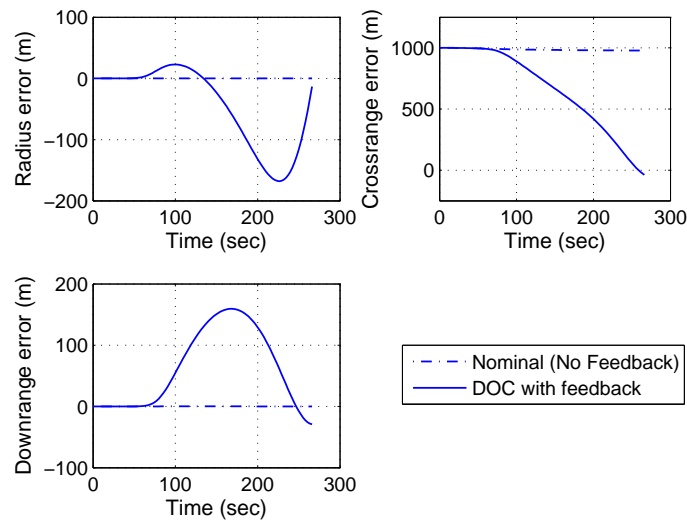


Figure 11: Time history of position errors, due to initial crossrange error of 1000m.

which will add more control authority and degree of freedom for the optimizer.

## 5 Conclusion

In this paper, DOC methodology is applied in an effort to develop an optimal (in terms of bank angle control energy) Mars EDL trajectory along which the landing precision has reduced sensitivity with respect to perturbations and uncertainties along the trajectory. It is assumed that the entry vehicles flies at a constant trim angle of attack, and the control of the entry trajectory is achieved through modulating the vehicle bank angle. Only the entry portion of the EDL trajectory from the atmospheric interface to the parachute deployment is considered, and the initial position error at the entry are considered as the only perturbations. It is shown in the paper that the DOC methodology is capable of reducing the target hitting error as a result of the initial position error. For the radius channel, the DOC methodology can reshape the nominal trajectory to achieve some level of sensitivity reduction, but for the downrange and crossrange channel, only through feedback control law can the sensitivity be reduced.

## References

- [1] Robert D. Braun and Robert M. Manning. Mars exploration entry, descent and landing challenges. *IEEE Aerospace Conference, Big Sky Montana, March 2006*.
- [2] Robert D. Braun, Richard W. Powell, F. McNeil Cheatwood, Spencer David A., and Robert A. Mase. The mars surveyor 2001 lander: A first step toward precision landing. *IAF 98-Q.3.03, 49th International Astronautical Congress, Sept. 28 - Oct. 2, 1998, Melbourne, Australia*.
- [3] Richard W. Powell. Numerical roll reversal predictor-corrector aerocapture and precision landing guidance algorithms for the mars surveyor program 2001 missions. *AIAA Atmospheric Flight Mechanics Conference, August 10-12, 1998, Boston, MA. AIAA 98-4574*.
- [4] Gilbert L. Carman, Dallas G. Ives, and David K. Geller. Apollo-derived mars precision lander guidance. *AIAA Atmospheric Flight Mechanics Conference, August 10-12, 1998, Boston, MA. AIAA 98-4570*.
- [5] L. E. Bryant, Tigges M. A., and D. G. Ives. Analytic drag control for precision landing and aerocapture. *AIAA Atmospheric Flight Mechanics Conference, August 10-12, 1998, Boston, MA. AIAA 98-4572*.

- [6] Munir Mohammad S. Tu, Kuang-Yang, Kenneth D. Mease, and David S. Bayard. Drag-based predictive tracking guidance for mars precision landing. *AIAA Atmospheric Flight Mechanics Conference, August 10-12, 1998, Boston, MA*. AIAA 98-4573.
- [7] David W. Way, Powell Richard W., Chen Allen, Adam D. Steltzner, A. Miguel San Martin, P. Daniel Burkhart, and Gavin F. Mendeck. Mars science laboratory: Entry, descent, and landing system performance. *IEEEAC paper #1467, version 3*, February 2006.
- [8] Mary Kae Lockwood, Richard W. Powell, Claude A. Graves, and Gilbert L. Carman. Entry system design considerations for mars landers. *24th Annual AAS Guidance and Control Conference, Jan. 31 - Feb. 4, 2001, Breckenridge, Colorado*. AAS 01-023.
- [9] H. Seywald and R.R. Kumar. Desensitized optimal trajectories. *Advances in the Astronautical Sciences, Spaceflight Mechanics 1996*, 93:103–116, 1996.
- [10] H. Seywald. Desensitized optimal trajectories with control constraints. *Advances in the Astronautical Sciences, Spaceflight Mechanics 2003*, 114:737–744, 2003.
- [11] H. Seywald. Desensitized optimal orbit insertion. *14th Space Flight Mechanics Meeting, 8-12 February, 2004, Maui, Hawaii*.
- [12] H. Seywald. Trajectory optimization based on differential inclusion. *Journal of Guidance, Control, and Dynamics*, 17(3):480–487, 1994.
- [13] C.R. Hargraves and S.W. Paris. Direct trajectory optimization using nonlinear programming and collocation. *Journal of Guidance*, 10(4):338–342, 1987.